THE JOURNAL OF PHYSICAL CHEMISTRY A

Article

pubs.acs.org/JPCA

Comparative Kinetics of the 3-Buten-1-ol and 1-Butene Reactions with OH Radicals: A Density Functional Theory/RRKM Investigation

Silvina Peirone,[†] Jorge D. Nieto,[†] Pablo M. Cometto,[†] Thaís da Silva Barbosa,[‡] Glauco Favilla Bauerfeldt,*[,‡] Graciela Arbilla,[§] and Silvia I. Lane[†]

[†]Instituto de Investigaciones en Fisicoquímica de Córdoba (INFIQC), Centro Láser de Ciencias Moleculares, Departamento de Fisicoquímica, Facultad de Ciencias Químicas, Universidad Nacional de Córdoba, Ciudad Universitaria, 5000 Córdoba, Argentina

[‡]Departamento de Química, Instituto de Ciências Exatas, Universidade Federal Rural do Rio de Janeiro, Seropédica, RJ 23851-970, Brazil

[§]Departamento de Físico-Química, Instituto de Química, Universidade Federal do Rio de Janeiro, Rio de Janeiro, RJ 21941-901, Brazil

Supporting Information

ABSTRACT: The compared kinetics of the reactions of unsaturated alcohols and alkenes with OH radicals is a topic of great interest from both the theoretical chemistry and the atmospheric chemistry points of view. The enhanced reactivity of an unsaturated alcohol, with respect to its alkene analogue, toward OH radicals has been previously demonstrated, at 298 K, by experimental and theoretical research. In this work, a new comparative investigation of such reactions is performed for 3-buten-1-ol and 1-butene. The model assumes that the overall kinetics is governed by the first OH addition steps of the mechanism. Calculations have been performed at the DFT level, employing the BHandHLYP functional and the cc-pVDZ and aug-cc-pVDZ basis sets, and the rate coefficients have been determined on the basis of the microcanonical variational transition state theory. The rate coefficients obtained for the OH reactions with 3-buten-1-ol (k_{OH}^{31BO}) and 1-butene (k_{OH}^{1B}) at 298.15 K are lower than the experimental rate coefficient available in the literature, showing deviations of 18% and 25%, respectively. Negative temperature dependence is verified for these rate coefficients. The $k_{OH}^{31BO}/k_{OH}^{1B}$ ratios have also been investigated as a function of the temperature, suggesting that at room temperature the unsaturated alcohol reacts with the OH radicals faster than 1-butene, by a factor of 1.2, but at higher temperatures (400−500 K), the alkene should react faster, and that the stabilization of prebarrier complexes and saddle points due to hydrogen bonds is no longer an important factor to govern the reactivity of the unsaturated alcohol toward OH radicals, with respect to the alkene analogue.

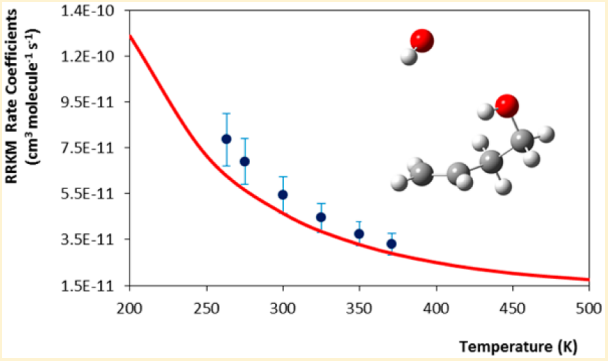

1. INTRODUCTION

The atmospheric chemistry of unsaturated hydrocarbons, especially alkenes, is widely known to be governed by the OH addition reactions and, at minor scale, reaction with ozone.[1] Several experimental reports concerning the kinetics of the alkenes + OH reactions are available in the literature, since the pioneer work in the 1970s. For 1-butene, for example, rate coefficients at room temperature have been determined by Morris and Niki and Pastrana and Carr,[2,3] while the temperature dependence of the rate coefficients has been reported by Atkinson and Pitts, in the range from 297−425 K, showing a negative temperature dependence.[4] Room-temperature rate coefficients have also been reported, in agreement with those previously determined,[5−9] and rate coefficients at lower temperatures for the OH addition reaction and at higher temperatures, for the hydrogen abstraction reaction, can also be found.[10−13] The OH addition mechanism is believed to prevail over the H-abstraction channels at room temperature,[14,15] the latter accounting for less than 10% of the overall rate coefficient.[16,17] The recommended rate coefficients for the 1-butene + OH reaction are expressed by the Arrhenius equation (280−420 K): $6.54 \times 10^{-12} \times \exp[3.89/RT]$, in which pre-exponential factor and activation energies are found in cm^3 molecule^{-1} s^{-1} and kJ mol^{-1} units, respectively.[16−18]

The unsaturated alcohols are also emitted into the troposphere, as primary pollutants, by both biogenic and anthropogenic sources. Among the volatile compounds, 3-buten-1-ol (31BO) is of particular interest, being applied as starting material for the synthesis of polymers. The room-temperature rate coefficient for the 31BO + OH reaction has been determined by Papagni and co-workers by the relative rate method as $(5.5 \pm 0.2) \times 10^{-12}$ cm^3 molecule^{-1} s^{-1}.[19] The

Received: December 16, 2014
Revised: March 17, 2015
Published: March 18, 2015

DOI: 10.1021/jp512544x
J. Phys. Chem. A 2015, 119, 3171−3180

temperature and pressure dependence of the rate coefficients for the 31BO + OH reaction have been experimentally determined, also showing a non-Arrhenius profile, with the rate coefficients fitted by the expression: $4.00 \times 10^{-12} \times \exp[6.51/RT]$ (263−371 K, in units of cm^3 $molecule^{-1}$ s^{-1} and kJ mol^{-1}).[20] Moreover, as it was pointed out by Cometto et al., the reactivity of this unsaturated alcohol toward the OH radical is nearly 2 times higher than that observed for 1-butene, at 298 K. In addition to the experimental papers, a theoretical work by Du and co-workers reports a complete potential energy surface investigation for the possible 31BO + OH reaction channels, at the QCISD(T)/6-311++G(d,p)//MP2(full)/6-311G(d,p) level.[21] As suggested, the OH reaction with unsaturated alcohols yields dialcohol radicals via the addition channel, with formation of a prebarrier complex (PC), stabilized by 6.4 kJ mol^{-1} in relation to the isolated reactants, which further converts to the addition products via a saddle point also located below the isolated reactants (with relative energies of 3.8 and 4.8 kJ mol^{-1}, for the reactions leading to the OH addition to terminal and central carbon atoms, respectively). To the best of our knowledge, no previous investigation concerning the prediction of rate coefficients for either 31BO or 1-butene, or the comparative kinetics of these compounds, is available in the literature.

In this work, the addition reactions of OH to 31BO and 1-butene are investigated, assuming the general reaction mechanism (A is 31BO or 1-butene, π-PC is the prebarrier complex, I_c and I_t are the products of the OH addition to the central and terminal carbon atoms, and, in parentheses, the k_i are the rate coefficients corresponding to each reaction step):

$$A + OH \rightarrow \pi\text{-PC} \qquad (k_1)$$

$$\pi\text{-PC} \rightarrow A + OH \qquad (k_{-1})$$

$$\pi\text{-PC} \rightarrow I_c \qquad (k_2(c))$$

$$\pi\text{-PC} \rightarrow I_t \qquad (k_2(t))$$

A similar mechanism has been successfully employed for the investigation of the OH addition reactions to 2-methyl-2-propen-1-ol and 2-methylpropene.[22] Here, our main goal is to investigate the relative reactivity of 31BO with respect to its alkene analogue, 1-butene, on the basis of potential energy profiles and rate coefficients calculations.

2. COMPUTATIONAL METHODS

The reactions have been described at the Density Functional Theory (DFT) level,[23] adopting the BHandHLYP functional[24] along with the cc-pVDZ (CCD) and the aug-cc-pVDZ (ACCD) basis sets.[25] The BHandHLYP has been pointed out as the functional that best reproduces the high accurate (and computational demanding) ab initio levels for H-abstraction reaction barriers,[26] molecular properties of diatomics with high electrostatic interactions, like NaCl,[27] and was also proved to perform similarly to the widely adopted B3LYP functional for the prediction of molecular properties of complexes of nonbonding interactions.[28] Moreover, in our previous work, the BHandHLYP functional was proved to show, for the OH addition to unsaturated compounds, a performance as good as the ab initio CCSD(T) and QCISD(T) methods.[22]

Geometry optimizations for all stationary points, including the saddle points, have been performed and vibrational frequencies have been further calculated, at the same theoretical levels, for the characterization of each stationary point. Spin contamination has been observed in all DFT calculations, and in all cases the value has been greater than 0.77. The minimum energy paths connecting the prebarrier complexes and addition products, passing through the corresponding saddle points, have been calculated using the intrinsic reaction path (IRC) method.[29] For the reaction path connecting the reactants to the prebarrier complexes, scan calculations over the C−OH interatomic distances have been employed. Thermochemical properties have been calculated using conventional Statistical Thermodynamics relations, assuming the harmonic oscillator, rigid rotor, and ideal gas models.[30] Theoretical calculations have been performed with the Gaussian 09 program.[31]

The primary addition of the OH radical to the unsaturated alcohol is expected to be a barrierless reaction, for which the conventional transition state theory should not apply and, instead, variational transition state methods are required.[32] The coefficients have been determined on the basis of the microcanonical variational transition state theory, over the temperature range 200−400 K. In our previous work, the adoption of the RRKM method has proved to be very important for an accurate prediction of the rate coefficients.[22] The calculations have been performed considering conservation of energy and angular momentum, for a range of energy values up to 210 kJ mol^{-1} and J quantum number values ranging from 0 to 200. The sums of states for the outer and inner transition states ($N_1(E,J)$ and $N_2(E,J)$ ($=N_2^{(c)}(E,J) + N_2^{(t)}(E,J)$, respectively)) have been calculated by a variational procedure allowing the location of the microcanonical transition states along each reaction path using the RRKM code.[33] From $N_1(E,J)$ and $N_2(E,J)$, the effective sums of states are calculated as

$$\frac{1}{N_{eff}(E,J)} = \left(\frac{1}{N_1(E,J)} + \frac{1}{N_2(E,J)} - \frac{1}{N_{max}}\right) \qquad (2)$$

N_{max} represents the maximum flux through the transition states, and the last term is, therefore, assumed to be negligible. This procedure is in accordance with the suggestion of Greenwald and co-workers, who stated that the canonical partition should not be expected for species stabilized by low energy values, such as the π-PC, even though the energy and angular momentum constrains must be respected.[34] The expression above assumes the ergodic hypothesis between the inner and outer transition states, with statistical probabilities of crossing a given transition state. The high pressure rate coefficients have been finally calculated by the integral:

$$k^{\infty}(T) = \sigma_r \frac{1}{hQ_A Q_{OH} Q_{rel}} \int g_J N_{eff}(E,J) \exp\left(-\frac{E}{k_B T}\right) dJ\, dE \qquad (3)$$

where σ_r, g_J, Q_A, Q_{OH}, and Q_{rel} are the reaction path degeneracy, the degeneracy of the rotational states, and the partition function for the unsaturated compound, A, for the OH, and the relative translational partition function, respectively. The Planck and Boltzmann constants are conventionally represented by h and k_B. In all rate coefficients calculations, the spin−orbit effect for the OH radical has been considered.

The contribution of possible reactants conformers to the global kinetics has also been investigated for the OH + 1-butene reaction, and the final rate coefficients have been calculated from the global rate coefficient found for each

DOI: 10.1021/jp512544x
J. Phys. Chem. A 2015, 119, 3171−3180

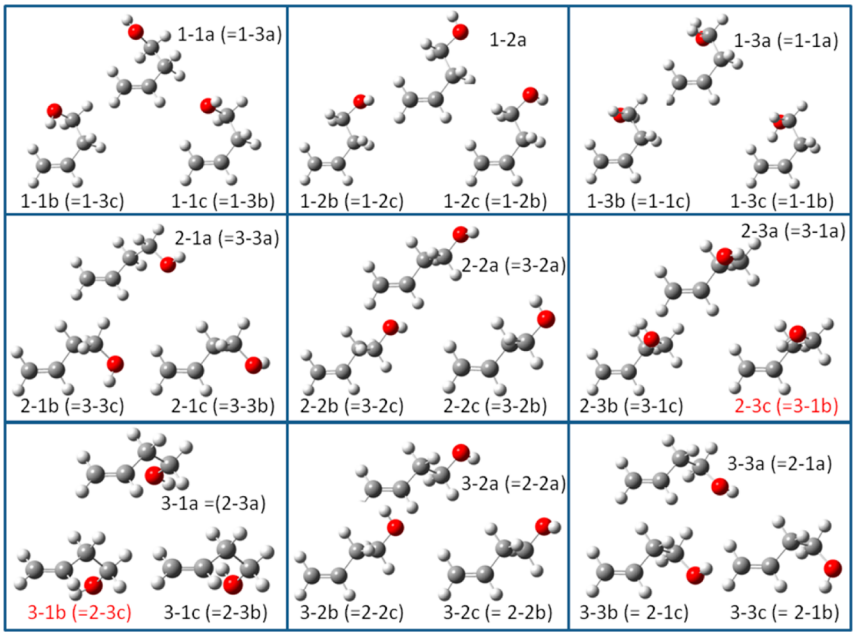

Figure 1. Conformers of 31BO, obtained at the BHandHLYP/aug-cc-pVDZ level (see text for details).

conformer and the population of the conformer, predicted as the Boltzmann distribution, at each temperature.

3. RESULTS AND DISCUSSION

3.1. The 31BO + OH Reaction. We begin our discussion by investigating the 31BO potential energy surface aiming to explore the possible conformers and rotamers of the reactant and the location of the minimum energy geometry. Therefore, scan calculations over the dihedral angles were performed at the BHandHLYP/ACCD level. Possible conformers can arise from the rotation of the three different torsion angles of the carbon atoms, C2 and C1, and the OH group, giving a total of 27 possible rotamers. After the location of the possible rotamers, from the scan calculations, the geometries were optimized and further characterized by vibrational frequencies calculations. Some groups of mirror images were identified, and a final ensemble of 14 distinct conformers was achieved.

A complete map of conformers is given in Figure 1, in which the conformers are labeled according to the rotating torsion angle: the first number refers to the rotation over the carbon atom C2 (which resulted in three possible conformers), the second number refers to the rotation over the carbon atom C1 (which resulted in three possible conformers for each initial conformer obtained by the rotation over C2), and the letter refers to the orientation of the hydrogen atom at the OH group (which resulted in three possible conformers for each conformer obtained by the rotation over C1). The global minimum, conformer 2-3c, is shown. The corresponding mirror image geometries are given in parentheses (note that reflection on the conformer 1-2a results in itself).

Populations regarding each conformer are calculated as a function of the temperature ($\mathrm{Pop}_i(T)$), according to the Boltzmann distribution:

$$\mathrm{Pop}_i(T) = \frac{\exp(-\Delta G_i(T)/RT)}{\sum \exp(-\Delta G_i(T)/RT)} \quad (4)$$

The minimum energy conformer is shown in Figure 1, and, by assuming eq 4, the population regarding this geometry varies from 60% to 20% as the temperature increases from 200 to 500 K. Each one of the other conformers contributes with less than 15% to the population. Populations, obtained at the BHandHLYP level with the CCD and ACCD basis sets for each conformer introduced in Figure 1, are given in Figure 2. As can be noted from Figure 2, the population is not sensitive to the quality of the basis set and varies significantly as a function of the temperature, as expected.

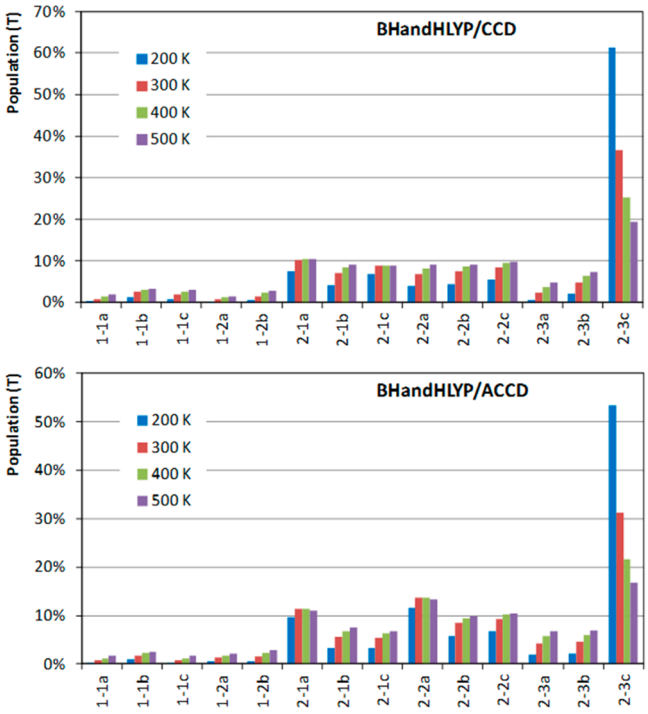

Figure 2. Populations, obtained for each conformer at the BHandHLYP level with the cc-pVDZ (CCD) and aug-cc-pVDZ (ACCD) basis sets, as a function of the temperature (K).

DOI: 10.1021/jp512544x
J. Phys. Chem. A 2015, 119, 3171−3180

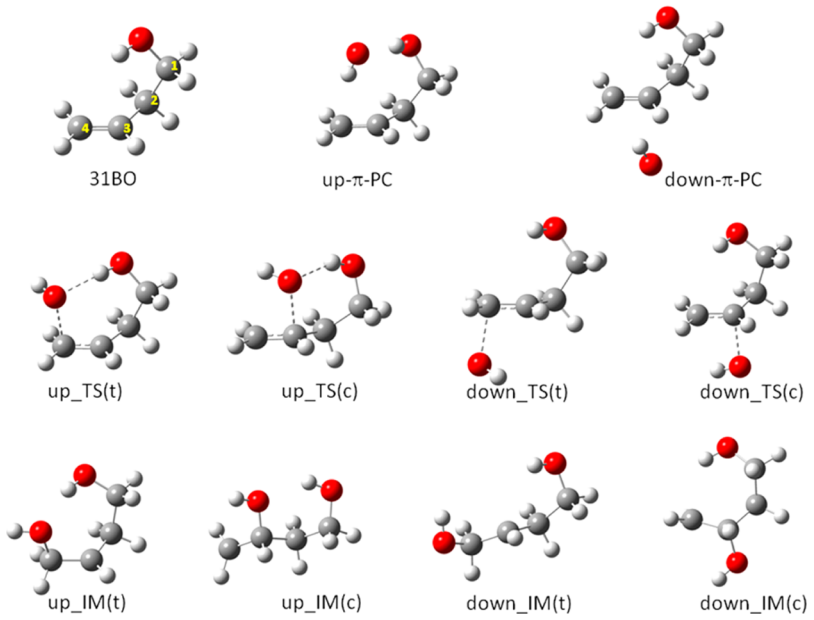

Figure 3. Structures for reactants, prebarrier complexes, saddle points, and products along the 31BO + OH reaction profile.

The minimum energy conformer of the 31BO (conformer 2-3c) shows the dihedral angles d_{HOC1C2} = 51.4°, $d_{OC1C2C3}$ = −65.1°, and $d_{C1C2C3C4}$ = 109.8° (the labels refer to the conventional IUPAC atom numbering). A mirror inversion of this structure reveals a nonsuperimposable conformer (an enantiomer). The HO, OC1, C1−C2, C2−C3, and C3═C4 distances are (in Å) 0.955, 1.408, 1.525, 1.497, and 1.328. A comparison of our geometry with the previously reported by Du and co-workers, obtained at the MP2(full)/6-311G(d,p) level,[21] shows good agreement for the interatomic distances (with root-mean-square deviation less than 0.01 Å), but apparently the dihedral angles significantly differ and the geometry reported by Du resembles one of our conformers, which contributes, at 298 K, with less than 7% to the total population.

We assume that the global reaction dynamics will be followed by the structures of the several stationary points (π-PCs, saddle points, and products) that can be connected, along the reaction paths, to that minimum energy conformation of the 31BO, keeping the same geometric and conformational profile of the global minimum.

The negative dependence of the rate coefficients with the temperature has been justified by a mechanism in which the reversible formation of a prebarrier complex takes place, followed by an irreversible reaction step through a saddle point, which is also located below the isolated reactants.[35−38] The prebarrier complex is generally a loosely bound structure, and can be classified as "sigma" (σ) or "pi" (π) types, whether the OH radical lies parallel or perpendicular to the plane that contains the double bond, respectively. Moreover, the π-type prebarrier complexes are stabilized with respect to the σ-type complexes, which can be justified by the noncovalent interaction of the H atom (from the OH radical) with the electronic density of the double bond. In the case of the OH addition to unsaturated alcohols, an additional electrostatic interaction between the O atom (from the OH radical) and the H atom (from the OH group of the alcohol) is expected, which stabilizes both σ- and π-type prebarrier complexes with respect to their analogues on the alkene + OH potential energy surface.[22] The energy difference between the σ- and π-type prebarrier complexes is relatively small (eventually, less than 1 kJ mol^{-1}), and the barrier to interconversion is assumed to be even smaller so that this process is expected to be fast (in the time scale of the global reaction) and the kinetics can be described by the formation/dissociation of the π-type complexes and its further reaction through the central barrier, neglecting therefore the σ-type complexes.

For the 31BO + OH reaction, two π-type prebarrier complexes (π-PCs) were located, corresponding to an upward and downward OH attack to the unsaturated alcohol (the "up" side of the molecule is assumed to be above the plane that contains the double bond, in which the $-CH_2-CH_2OH$ moiety is located; see Figure 3). These structures are remarkably distinct, because the above-mentioned additional electrostatic interactions that stabilize the π-PC on the unsaturated alcohol + OH potential energy surface are only observed on the up-π-PC. The energy difference, corrected by zero-point vibrational energy, between the up-π-PC and down-π-PC is 5.11 kJ mol^{-1} at the BHandHLYP/ACCD level. Also worth comparing are the relative energies of our up-π-PC and of the prebarrier complex reported by Du and co-workers,[21] which is, as mentioned above, −6.4 kJ mol^{-1}, whereas ours is stabilized by 11.09 kJ mol^{-1}.

Regarding the geometric parameters obtained at the BHandHLYP/ACCD level, the up-π-PC and down-π-PC show the hydrogen atom of the OH radical oriented to the allylic plane, with dihedral angles $d_{O(OH)C4C3C2}$ = −102.3° and $d_{O(OH)C4C3C2}$ = 89.3°, respectively. The oxygen−carbon bond distances are 3.347 Å ($O^{(OH)}$−C4) and 3.297 Å ($O^{(OH)}$−C3) for the up-π-PC and 3.491 Å ($O^{(OH)}$−C4) and 3.366 Å ($O^{(OH)}$−C3) for the down-π-PC. No significant changes are verified for the C3C4 double bond distance or OH (from the alcohol) at the π-PCs with respect to that at the 31BO, the C3C4 double bond distance being 1.328 Å at the isolated unsaturated alcohol and 1.328 and 1.330 Å at the up-π-PC and down-π-PC, respectively, and the OH bond distance being 0.955 Å at the isolated unsaturated alcohol and 0.957 and 0.954 Å at the up-π-PC and down-π-PC, respectively. The bond

DOI: 10.1021/jp512544x
J. Phys. Chem. A 2015, 119, 3171−3180

distance at the OH radical (0.966 Å) is slightly increased at the π-PCs, being 0.972 Å at the up-π-PC and 0.970 at the down-π-PC.

The geometry reported by Du and co-workers[21] does not suggest any interaction of the OH radical with the OH functional group in 31BO; likewise, our down-π-PC also does not show such interactions. In our up-π-PC, the opposite is observed, the oxygen atom (from the OH radical) interacting with the hydrogen atom (from the alcohol group) with an interatomic distance of 2.044 Å. That is probably the reason for the differences in the relative energy of that π-PC previously reported and of our up-π-PC. In fact, the relative energy of Du's π-PC calculated at the QCISD(T)/6-31++G(d,p)//MP2/6-311G(d,p) level well agrees with the relative energy of our down-π-PC, at the BHandHLYP/ACCD level, −5.98 kJ mol^{-1}.

The reaction profile connecting the prebarrier complexes to the isolated reactants was described by a potential curve in which, starting from each π-PC, the $O^{(OH)}$−C3 distances was increased up to 10 Å, leading to the isolated reactants. At this point, the final energy observed on the potential curve showed reasonable agreement with the sum of the electronic energies of the isolated reactants.

The saddle points for the OH upward addition to the central and terminal carbon atoms, up_TS(c) and up_TS(t), are also located below the reactants, stabilized by 5.02 and 5.10 kJ mol^{-1}, respectively, at the BHandHLYP/ACCD level. Like at the up-π-PC, these TSs also show an interaction between the oxygen atom (from the OH radical) and the hydrogen atom (from the alcohol group) with interatomic distances of 1.882 Å (up_TS(c)) and 1.911 Å (up_TS(t)). The geometries for up_TS(c) and up_TS(t) resemble cyclic structures with six- and seven-membered rings, respectively. The O−C interatomic distances are 2.156 Å (O−C3, up_TS(c)) and 2.172 Å (O−C4, up_TS(t)). Another important geometric feature is found at the C3C4 double bond distance, which is increased at the up-TSs with respect the optimized values at the 31BO and up-π-PCs, being 1.357 Å (C3C4, up_TS(c)) and 1.353 Å (C3C4, up_TS(t)).

The saddle points for the downward addition to the central and terminal carbon atoms, down_TS(c) and down_TS(t), show electronic energies smaller than those of the isolated reactants, although the inclusion of zero-point vibrational energy leads to positive relative energies of 3.39 and 3.77 kJ mol^{-1}, at the BHandHLYP/ACCD level. As at the down-π-PC, the down-TSs do not show any interaction between OH groups. The O−C interatomic distances are 2.100 Å (O−C3, down_TS(c)) and 2.123 Å (O−C4, down_TS(t)), slightly smaller than the corresponding values at the up-TSs, and the C3C4 distances are 1.357 Å (up_TS(c)) and 1.352 Å (up_TS(t)).

Starting from each saddle point, IRC calculations were performed for the description of the reaction profiles leading to the formation of the dialcohol radicals resulting from the addition of the hydroxyl radical to either the central or the terminal carbon atoms, from upward and downward attacks.

Along the reaction path, the structural changes experienced by the elongation of the C3C4 and decrease of the O−C distances are evident, yielding the dialcohol radicals, hereafter referred as IM(c) and IM(t), respectively. Note that the products up_IM(c) and down_IM(c), resulting from the reaction paths starting from the up-π-PC and down-π-PC and passing through the up_TS(c) and down_TS(c), are rotamers of the IM(c), as well as the products up_IM(t) and down_IM(t) are rotamers of the IM(t). Other rotamers of the IM(c) and IM(t) radicals can be found. However, attempts to locate other geometries for the rotamers of the saddle points failed.

The structures for the prebarrier complexes, saddle points, and products, obtained at the BHandHLYP/ACCD level, are shown in Figure 3. Molecular properties (including optimized geometries, vibrational frequencies, and electronic energies) for all stationary points obtained at the BHandHLYP/ACCD level are given as Supporting Information. The summarized relative energies obtained at the BHandHLYP level with the CCD and ACCD basis sets are introduced in Table 1.

Table 1. Relative Energies (With Respect to the Isolated Reactants, Expressed in kJ mol^{-1}) for Several Stationary Points along the 31BO + OH Reaction Path, Calculated at the BHandHLYP Level with the cc-pVDZ (CCD) and aug-cc-pVDZ (ACCD) Basis Sets

	CCD		ACCD	
BHandHLYP	ΔE	ΔE^{oa}	ΔE	ΔE^{oa}
31BO + OH	0.00	0.00	0.00	0.00
up-π-PC	−30.67	−23.97	−16.99	−11.09
up_TS(t)	−23.39	−13.64	−14.56	−5.10
up_TS(c)	−23.01	−13.81	−14.35	−5.02
up_IM(t)[b]	−139.72	−135.06	−125.84	−121.30
up_IM(c)[b]	−133.53	−129.92	−122.87	−119.38
down-π-PC	−13.26	−8.62	−10.84	−5.98
down_TS(t)	−0.75	5.23	−2.68	3.77
down_TS(c)	−4.73	1.59	−2.84	3.39
down_IM(t)[b]	−120.16	−116.50	−115.76	−112.21
down_IM(c)[b]	−115.32	−112.30	−110.25	−107.14

[a]Relative energies corrected by zero-point vibrational energies. [b]The relative energies of the minimum energy rotamer of the group are reported in this table.

3.2. The 1-Butene + OH Reaction. The 1-butene molecule shows three conformers, 1B_1, 1B_2, and 1B_3, with 1B_3 being a mirror image of 1B_1 and 1B_2 and 1B_1 separated by 1.44 kJ mol^{-1}, at the BHandHLYP/ACCD level (or 1.50 kJ mol^{-1}, at the BHandHLYP/CCD level). The dihedral angles, $d_{C1C2C3C4}$, of the 1B_1 and 1B_2 conformers are 120.3° and 0.0°, respectively. Staring from these two geometries, prebarrier complexes, saddle points, and addition products were located at the BHandHLYP level, with both CCD and ACCD basis sets. Because of symmetry, the π-PCs and TSs resulting from the OH upward and downward attacks to the 1B_2 conformer are indistinguishable, although distinct saddle points for the addition to the central and terminal carbon atoms must be considered. Thus, for the 1B_1, an addition mechanism similar to that proposed for 31BO + OH reaction, explicitly considering the upward and downward OH attacks, is proposed, whereas for the 1B_2 conformer, the kinetics was evaluated from the simplified mechanism (in which the upward and downward OH attacks are the same). The overall kinetics is supposed to be a contribution of the individual global rate coefficients obtained for each conformer.

The geometries of the stationary points, including the prebarrier complex and saddle points, are shown in Figure 4. The relative energy values with respect to the isolated reactants are summarized in Table 2.

Because the computational procedures adopted for the description of the 31BO + OH reaction were also employed for

DOI: 10.1021/jp512544x
J. Phys. Chem. A 2015, 119, 3171−3180

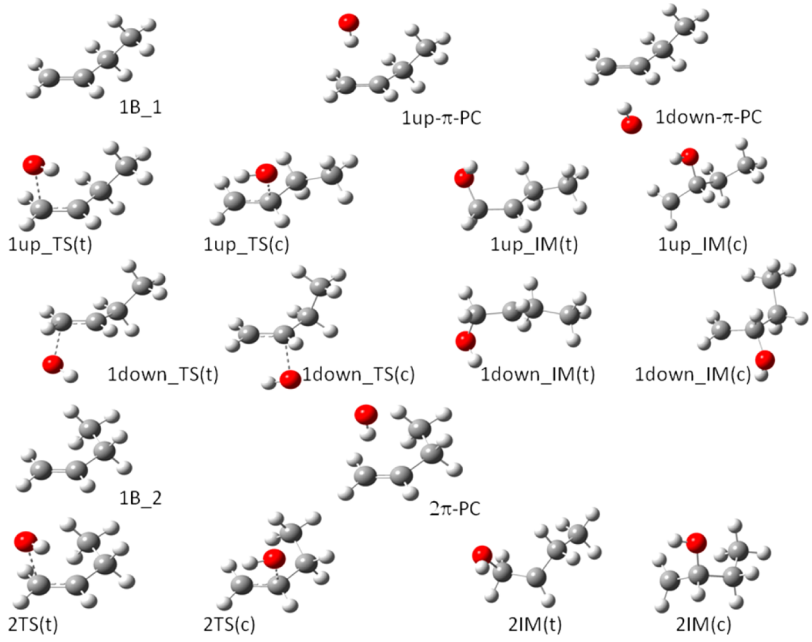

Figure 4. Structures for reactants, prebarrier complexes, saddle points, and products along the 1-butene + OH reaction profile.

Table 2. Relative Energies (With Respect to the Isolated Reactants, Expressed in kJ mol^{-1}) for Several Stationary Points along the 1-Butene + OH Reaction Path, Calculated at the BHandHLYP Level with the cc-pVDZ (CCD) and aug-cc-pVDZ (ACCD) Basis Sets

	CCD		ACCD	
BHandHLYP	ΔE	$\Delta E^{\circ a}$	ΔE	$\Delta E^{\circ a}$
1B_1 + OH	0.00	0.00	0.00	0.00
1up-π-PC	−21.50	−15.19	−13.35	−7.95
1up_TS(t)	−8.46	−0.46	−6.60	0.50
1up_TS(c)	−5.90	0.67	−3.80	2.72
1up_IM(t)	−125.12	−108.92	−118.69	−103.24
1up_IM(c)	−124.37	−110.54	−119.04	−105.46
1down-π-PC	−18.83	−12.93	−12.84	−7.74
1down_TS(t)	−4.55	2.22	−5.88	0.84
1down_TS(c)	−5.59	1.09	−4.92	1.63
1down_IM(t)	−125.12	−108.92	−118.69	−103.24
1down_IM(c)	−121.46	−108.08	−116.19	−103.11
1B_2^{b} + OH	0.75	1.50	0.58	1.44
2π-PC^{b}	−20.67	−14.60	−13.59	−8.40
2TS(t)^{b}	−7.54	−0.21	−6.84	0.17
2TS(c)^{b}	−7.23	−0.97	−5.76	0.94
2IM(t)^{b}	−124.29	−108.19	−117.20	−101.83
2IM(c)^{b}	−122.34	−108.97	−116.70	−103.56

^{a}Relative energies corrected by zero-point vibrational energies. ^{b}The 1B_2 energy is reported relative to the global minimum (1B_1), while the energies of the π-PC, TS(t), TS(c), IM(t), and IM(c) are reported relative to the 1B_2 + OH energy.

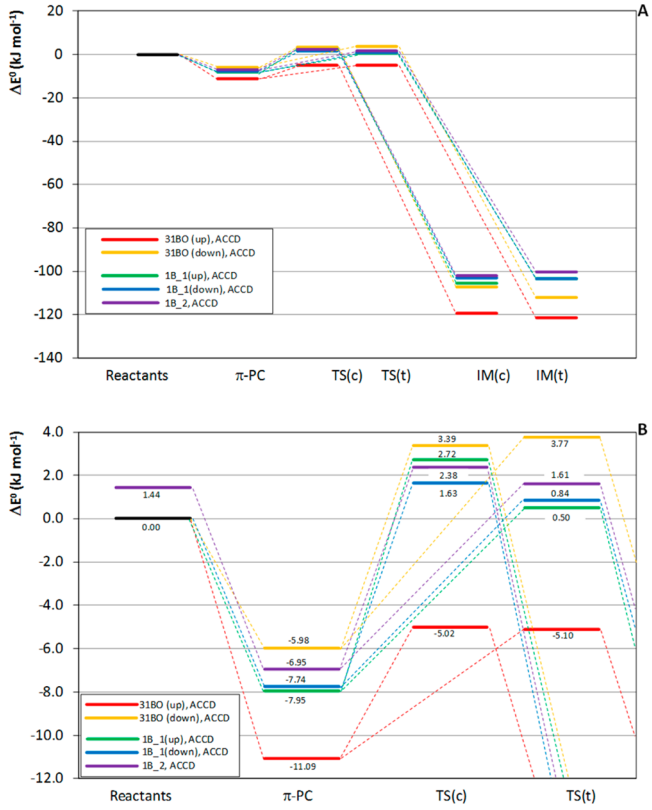

Figure 5. (A) Energy profiles for the 31BO + OH and 1-butene + OH reactions; (B) energy profiles for the 31BO + OH and 1-butene + OH reactions, enlarged at the π-PC and TS regions. Zero-point vibrational energy corrections are included.

the investigation of the 1-butene + OH reaction and general observations are also very similar, a detailed discussion is omitted. However, a brief highlight concerning the differences found for these reactions is necessary. In Figure 5 is introduced a comparison of the energy profiles for the 31BO + OH and 1-butene + OH reactions. First, the OH upward attack to 31BO results in the most stabilized prebarrier complex and saddle points, due to hydrogen-bond interaction between the oxygen atom from the OH radical and the hydrogen atom from the HO− group in 31BO, and no significant distinction can be observed between the relative energies calculated for these central or terminal saddle points, suggesting competitive channels, without prevalence of any addition. Contrary to the expectations, the OH downward addition to 31BO results in the less stabilized prebarrier complex and saddle points, and all

DOI: 10.1021/jp512544x
J. Phys. Chem. A 2015, 119, 3171−3180

prebarrier complexes and saddle points found for the 1B + OH reaction lie in between. The barrier heights for the π-PC → IM on the 1B potential energy surface are, however, similar to the down-π-PC → down-IM(c) (and down-IM(t)), as expected because the most significant contribution to the decrease of the energy of the system is absent at these structures. The barrier to the downward OH addition to the terminal carbon atom at the 31BO is slightly higher than that of the addition to the central carbon, and an inverse situation is found for the OH addition to 1B. Nevertheless, the differences for the barrier heights are still not enough to expect any prevalence of a particular addition channel.

3.3. Rate Coefficients for the 31BO + OH Reaction. A total of 20 points along the potential curves representing the dissociation reactions π-PC → 31BO + OH (up and down) and along each potential curve for the reactions π-PC → I (central and terminal, up and down) were used to evaluate the rate coefficients. Table 3 introduces the resulting rate coefficients in the range 200−500 K. The negative temperature dependence is also observed. As expected, mCVT/BHandHLYP/ACCD rate coefficients are lower than those calculated at the mCVT/BHandHLYP/CCD level. At 298 K, the calculated rate coefficients are 1.51×10^{-10} and 4.70×10^{-11} cm^3 molecule^{-1} s^{-1} (at mCVT/BHandHLYP/CCD and mCVT/BHandHLYP/ACCD levels, respectively), the latter in good agreement with the experimental value.[20]

Table 3. Microcanonical Variational Rate Coefficients k_{up}, k_{down}, and k_{global} (cm^3 molecule^{-1} s^{-1}), Calculated at the BHandHLYP Level with the cc-pVDZ (CCD) and aug-cc-pVDZ (ACCD) Basis Sets for the Upward and Downward OH Attacks to 3-Buten-1-ol, as a Function of the Temperature (T, in K)

	T (K)	k_{up}	k_{down}	k_{global}
CCD	200	3.20×10^{-10}	7.85×10^{-12}	3.28×10^{-10}
	250	2.17×10^{-10}	5.52×10^{-12}	2.26×10^{-10}
	300	1.44×10^{-10}	4.69×10^{-12}	1.49×10^{-10}
	350	9.49×10^{-11}	4.37×10^{-12}	9.93×10^{-11}
	400	6.38×10^{-11}	4.27×10^{-12}	6.81×10^{-11}
	450	4.41×10^{-11}	4.29×10^{-12}	4.84×10^{-11}
	500	3.16×10^{-11}	4.39×10^{-12}	3.60×10^{-11}
ACCD	200	9.40×10^{-11}	2.97×10^{-11}	1.24×10^{-10}
	250	5.40×10^{-11}	1.75×10^{-11}	7.15×10^{-11}
	300	3.35×10^{-11}	1.29×10^{-11}	4.63×10^{-11}
	350	2.21×10^{-11}	1.07×10^{-11}	3.28×10^{-11}
	400	1.55×10^{-11}	9.50×10^{-12}	2.50×10^{-11}
	450	1.14×10^{-11}	8.90×10^{-12}	2.03×10^{-11}
	500	8.90×10^{-12}	8.65×10^{-12}	1.76×10^{-11}

Figure 6 shows the mCVT (obtained from molecular properties and energies predicted at the BHandHLYP/aug-cc-pVDZ level) and the experimental rate coefficients, represented in an Arrhenius plot. It can be noted that the mCVT/BHandHLYP/ACCD rate coefficients agree very well with the experimental values, with deviations of less than 20%.

These rate coefficients can be finally expressed by the equation (the parameters are in units of cm^3 molecule^{-1} s^{-1} and kJ/mol):

$$k(T) = 0.44 \times 10^{-11} \exp\left(\frac{5.87}{RT}\right)$$

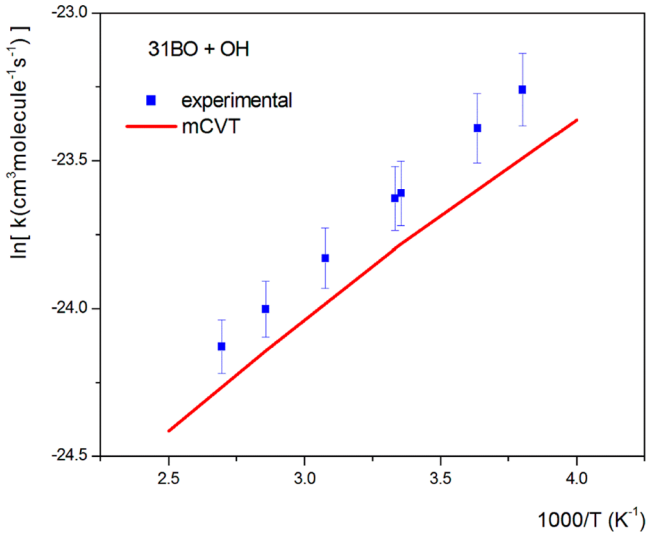

Figure 6. Microcanonical variational rate coefficients (cm^3 molecule^{-1} s^{-1}) calculated for the 31BO + OH reaction, obtained at the BHandHLYP/aug-cc-pVDZ level, as a function of the temperature (K). The experimental rate coefficients, taken from ref 20, are included for comparison.

in very good agreement with the experimental Arrhenius equation,[20] as shown in Figure 6. There are two points to be highlighted: first, the best agreement among the mCVT and experimental rate coefficients found not only at 298 K, but also at other temperature values and the Arrhenius parameters, suggesting that the mCVT model is very important for the description of the overall kinetics of the OH addition to 31BO. The second point is that the mCVT values are very close to the experimental values, despite that all of the calculations have been performed for only one conformer of the 31BO. Therefore, the good agreement between the calculated and experimental values also suggests that similar rate coefficient values may be expected for the other conformers, so that the overall rate coefficients, calculated as mean values of all of the rate coefficients found for all conformers, weighted by the corresponding Boltzmann populations at each temperature, should not be significantly different from the rate coefficients found for the 2-3c conformer. An even more important fact is that the kinetic model is very satisfactory for the description of the OH + 31BO reaction, and the inclusion of other conformers should represent, at this point, a less important refinement.

3.4. The OH Reaction with the Alkene and the Unsaturated Alcohol: Comparative Kinetics. Because both conformers of 1-butene should contribute to the reaction kinetics, a detailed mechanism considering these two starting points was considered. Moreover, the stationary points show nonsuperimposable mirror images, and each reaction degeneracy is assumed to be 2.

At the mCVT/BHandHLYP/ACCD level, the calculated rate coefficient at 298 K, 3.95×10^{-11} cm^3 molecule^{-1} s^{-1}, is in good agreement with the experimental value.[18] Table 4 introduces the resulting rate coefficients in the range 200−500 K. Branching ratios calculated for $k^{(1)}_{up}$, $k^{(1)}_{dwn}$, and $k^{(2)}$g, as a function of the temperature, are shown in Figure 7.

Calculated results show that $k^{(1)}_{down}$ contributes 58% to the global rate coefficient, while $k^{(1)}_{up}$ and $k^{(2)}$g represent 35% and 7% of the global rate coefficient, respectively. Moreover, the

DOI: 10.1021/jp512544x
J. Phys. Chem. A 2015, 119, 3171−3180

Table 4. Microcanonical Rate Coefficients (cm^3 $molecule^{-1}$ s^{-1}), Calculated at the BHandHLYP Level with the cc-pVDZ (CCD) and aug-cc-pVDZ (ACCD) Basis Sets for the OH Reaction with the Conformers 1B_1 and 1B_2 of 1-Butene, as a Function of the Temperature (T, in K)

		mCVT				
	T (K)	$k^{(1)}_{up}$	$k^{(1)}_{down}$	$k^{(1)}_{g}$	$k^{(2)}_{g}$	k_g
CCD	200	9.76×10^{-12}	6.91×10^{-12}	1.67×10^{-11}	2.23×10^{-11}	1.74×10^{-11}
	250	6.40×10^{-12}	5.35×10^{-12}	1.18×10^{-11}	1.49×10^{-11}	1.22×10^{-11}
	300	4.93×10^{-12}	4.67×10^{-12}	9.60×10^{-12}	1.15×10^{-11}	9.91×10^{-12}
	350	4.18×10^{-12}	4.39×10^{-12}	8.57×10^{-12}	9.74×10^{-12}	8.77×10^{-12}
	400	3.79×10^{-12}	4.31×10^{-12}	8.10×10^{-12}	8.78×10^{-12}	8.22×10^{-12}
	450	3.59×10^{-12}	4.35×10^{-12}	7.94×10^{-12}	8.25×10^{-12}	8.00×10^{-12}
	500	3.51×10^{-12}	4.48×10^{-12}	7.99×10^{-12}	7.98×10^{-12}	7.99×10^{-12}
ACCD	200	4.09×10^{-11}	6.98×10^{-11}	1.11×10^{-10}	4.28×10^{-11}	1.01×10^{-10}
	250	2.33×10^{-11}	3.94×10^{-11}	6.27×10^{-11}	2.47×10^{-11}	5.69×10^{-11}
	300	1.62×10^{-11}	2.72×10^{-11}	4.34×10^{-11}	1.72×10^{-11}	3.91×10^{-11}
	350	1.27×10^{-11}	2.12×10^{-11}	3.39×10^{-11}	1.35×10^{-11}	3.04×10^{-11}
	400	1.09×10^{-11}	1.80×10^{-11}	2.89×10^{-11}	1.15×10^{-11}	2.58×10^{-11}
	450	9.80×10^{-12}	1.62×10^{-11}	2.60×10^{-11}	1.03×10^{-11}	2.32×10^{-11}
	500	9.18×10^{-12}	1.51×10^{-11}	2.43×10^{-11}	9.61×10^{-12}	2.16×10^{-11}

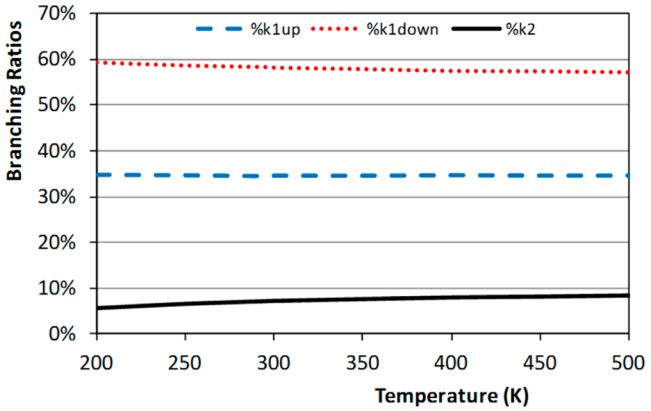

Figure 7. Branching ratios for the mCVT $k^{(1)}_{up}$, $k^{(1)}_{down}$, and $k^{(2)}_{g}$ rate coefficients for the 1B + OH reaction, as a function of the temperature (K).

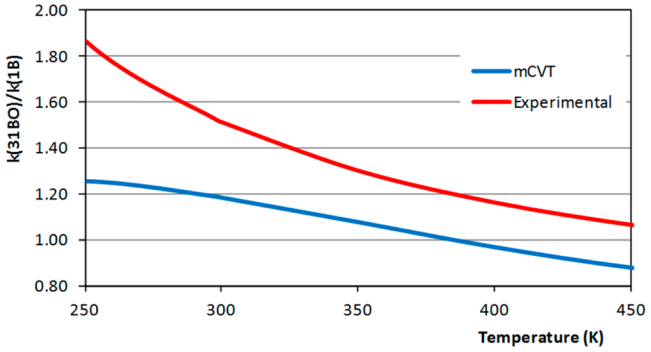

Figure 8. Microcanonical variational rate coefficients (cm^3 $molecule^{-1}$ s^{-1}) calculated for the 1B + OH reaction, obtained at the BHandHLYP/aug-cc-pVDZ level, as a function of the temperature (K). The experimental rate coefficients, taken from ref 4, are included for comparison.

calculated rate coefficients decrease as the temperature increases and follow the expression (the parameters are in units of cm^3 $molecule^{-1}$ s^{-1} and kJ/mol):

$$k(T) = 0.71 \times 10^{-11} \exp\left(\frac{4.33}{RT}\right)$$

Calculated mCVT rate coefficients for the 1B + OH reaction, in comparison with the experimental values (including the reported experimental error),[4] are shown in Figure 8.

The mCVT/BHandHLYP/ACCD rate coefficients for the 1B + OH reaction are overestimated, with respect to the experimental values, by almost 11% in the range 250−450 K. At the same temperature range, the mCVT/BHandHLYP/ACCD rate coefficients for the 31BO + OH reaction are underestimated by almost 18%. Despite this inverted behavior, the rate coefficients for the 31BO + OH can be compared to those for 1B + OH reaction, showing that at lower temperature values, the unsaturated alcohol reacts faster with the OH radicals than the alkene. At 298 K, for example, the calculated $k_{OH}^{31BO}/k_{OH}^{1B}$ ratio is 1.19, whereas the experimental data suggest the same ratio as 1.52. As the temperature increases, the $k_{OH}^{31BO}/k_{OH}^{1B}$ ratio decreases, and an inverted reactivity is predicted to be found at 400 K, with the value 0.97. At this temperature, the reactivity of the alcohol is nearly the same as the reactivity of the alkene toward the OH radicals, and, with further increase of the temperature, the alkene should react faster. Unfortunately, there are no experimental data to support this theoretical prediction (although the extrapolation of the experimental Arrhenius expressions for the alcohol and alkene reactions with OH suggests that the inversion of reactivity must occur at 500 K). The calculated and experimental $k_{OH}^{31BO}/k_{OH}^{1B}$ ratios are shown in Figure 9. In this figure, the experimental ratios as a function of the temperature are calculated on the basis of the Arrhenius expressions obtained for the experimental rate coefficients,[4,20] and the error bars are estimated by propagation of uncertainties of the reported Arrhenius parameters.

To justify the inversion of reactivity and search for the factors driving the kinetics of the OH reactions with the unsaturated alcohol and the alkene analogue, the kinetics of the upward and downward OH additions to 31BO may be analyzed and compared. At lower temperatures, the kinetics of the 31BO + OH reaction is dominated by the upward channel, where the stationary points (π-PC and saddle points) are most stabilized by hydrogen bonds. As the temperature increases, however, the contribution of the downward channel increases, showing that the stabilization due to hydrogen bonds is no longer the most

DOI: 10.1021/jp512544x
J. Phys. Chem. A 2015, 119, 3171−3180

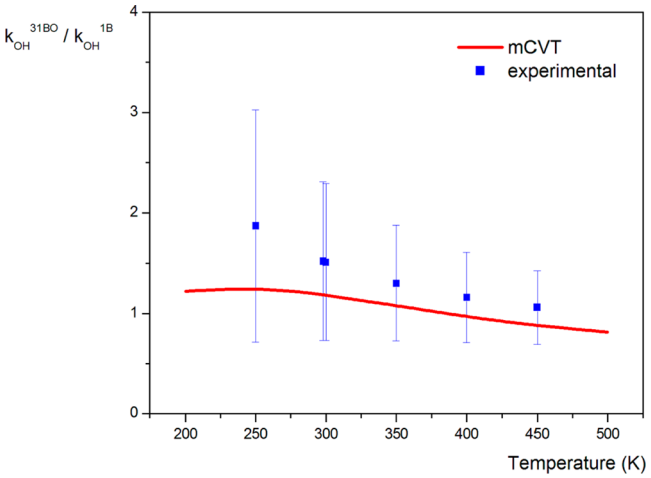

Figure 9. $k_{OH}^{31BO}/k_{OH}^{1B}$ ratio, as a function of the temperature (K). Experimental data taken from refs 4 and 20.

important factor governing the OH addition kinetics. Indeed, at high temperature values, the stabilization of the π-PC and saddle points of the 31BO + OH system is no longer the most important factor to govern the reactivity of the unsaturated alcohol with respect to its alkene analogue.

4. CONCLUSIONS

In this work, the rate coefficients for the reactions of OH radical with 3-buten-1-ol (31BO) and 1-butene (1B) have been calculated at the variational microcanonical transition state level, on the basis of potential energy surface results, obtained at the BHandHLYP level. The dynamics of the OH addition to the unsaturated compounds is described by the initial formation of a π-type prebarrier complex, which further results in an addition intermediate passing through a saddle point. The OH functional group plays a fundamental role in the stabilization of some of the prebarrier complexes, intermediates, and saddle points on the 31BO + OH potential energy surface.

The calculated rate coefficient for the 3-buten-1-ol + OH reaction at 298.15 K, adopting the microcanonical variational transition state method, is 4.70×10^{-11} cm^3 molecule^{-1} s^{-1} at the BHandHLYP/aug-cc-pVDZ level, whereas for the 1-butene, the calculated rate coefficient at 298.15 K is 3.95×10^{-11} cm^3 molecule^{-1} s^{-1}. The kinetics of the 1-butene was assumed to be a contribution of the several reaction steps undergone by each of the expected conformers of that molecule, populated according to the Boltzmann distribution. The overall result was satisfactory, with deviation from the experimental values of less than 25% (250−450 K). Both reactions show non-Arrhenius behavior, confirming the experimental observation.

The ratios of the rate coefficients for the 3-buten-1-ol + OH and 1-butene + OH reactions ($k_{OH}^{31BO}/k_{OH}^{1B}$ ratios) have also been investigated as a function of the temperature, suggesting that at room temperature the unsaturated alcohol reacts with the OH radicals faster than 1-butene, by a factor of 1.2. The enhanced reactivity of the alcohol with respect to the alkene analogue at room temperature is justified by the stabilization of prebarrier complexes and saddle points due to hydrogen bonds. At higher temperatures (400−500 K), however, the alkene reacts faster, and the hydrogen bonds are no longer an important factor to govern the reactivity of the unsaturated alcohol toward OH radicals, with respect to the alkene analogue. The kinetic models for both reactions have considered upward and downward OH additions and, eventually, multiconformational reaction paths, and it was shown that the rate coefficients for the OH addition passing through stationary point, which are stabilized by hydrogen bonds (the k_{up} rate coefficients for the 3-buten-1-ol reaction), decrease faster that those calculated for the reaction paths passing through the non stabilized stationary points (as the k_{down} rate coefficients for the 3-buten-1-ol reaction and the rate coefficients for the 1-butene reaction), and, as an overall result, the global rate coefficients for the 1-butene become higher than the rate coefficients for the 3-buten-1-ol reaction. Although these findings should not have significant atmospheric implications, they are very important for the understanding of the kinetics of the OH addition to unsaturated compounds.

The good agreement of our theoretical results with the experimental data contributes to the validation of the theoretical methodology for calculating rate coefficients for reactions of unsaturated compounds with OH radicals. This methodology may also be extended and recommended for the theoretical prediction to any other reaction passing through a slightly bonded prebarrier complex leading, through a saddle point, to a strongly stabilized reaction intermediate, or product.

■ ASSOCIATED CONTENT

Supporting Information

Geometric parameters (Å and deg), vibrational frequencies (cm^{-1}), and total energies (hartrees) for all stationary points. This material is available free of charge via the Internet at http://pubs.acs.org.

■ AUTHOR INFORMATION

Corresponding Author

*E-mail: bauerfeldt@ufrrj.br.

Notes

The authors declare no competing financial interest.

■ ACKNOWLEDGMENTS

We thank the Brazilian National Council for Scientific and Technological Development, CNPq (PROSUL, Proc. 490252/2011-7), and CONICET, ANPCyT-FONCyT, MinCyT, and SECyT-UNC of Argentina for financial support of this research, and the Coordination for the Improvement of Higher Education Personnel (CAPES), for a doctoral fellowship of T.S.B.

■ REFERENCES

(1) Seinfeld, J. H.; Pandis, S. N. *Atmospheric Chemistry and Physics: From Air Pollution to Climate Change*; Wiley: New York, 2006.
(2) Morris, E. D., Jr.; Niki, H. Reactivity of Hydroxyl Radicals with Olefins. *J. Phys. Chem.* **1971**, *75*, 3640−3641.
(3) Pastrana, A. V.; Carr, R. W., Jr. Kinetics of the Reaction of Hydroxyl Radicals with Ethylene, Propylene, 1-butene, and Trans-2-butene. *J. Phys. Chem.* **1975**, *79*, 765−770.
(4) Atkinson, R.; Pitts, J. N., Jr. Rate Constants for the Reaction of OH Radicals with Propylene and the Butenes Over the Temperature Range 279−425 K. *J. Chem. Phys.* **1975**, *63*, 3591−3595.
(5) Davis, D. D. Investigation of Important Hydroxyl Radical Reactions in the Perturbed Troposhere. EPA-600/3-77-11, 1977.
(6) Ravishankara, A. R.; Wagner, S.; Fischer, S.; Smith, G.; Schiff, R.; Watson, R. T.; Tesi, G.; Davis, D. D. A Kinetics Study of the Reactions of OH with Several Aromatic and Olefinic Compounds. *Int. J. Chem. Kinet.* **1978**, *10*, 783−804.

DOI: 10.1021/jp512544x
J. Phys. Chem. A 2015, 119, 3171−3180

(7) Nip, W. S.; Paraskevopoulos, G. Rates of OH Radical Reactions. VI. Reactions with C_3H_6, 1-C_4H_8 and l-C_5H_{10} at 297 K. *J. Chem. Phys.* **1979**, *71*, 2170−2174.
(8) Biermann, H. W.; Harris, G. W.; Pitts, J. N., Jr. Photoionization Mass Spectrometer Studies of the Collisionally Stabilized Product Distribution in the Reaction of Hydroxyl Radicals with Selected Alkenes at 298 K. *J. Phys. Chem.* **1982**, *86*, 2958−2964.
(9) Atkinson, R.; Aschmann, S. M. Rate Constants for the Reaction of OH Radicals with a Series of Alkenes and Dialkenes at 295 ± 1 K. *Int. J. Chem. Kinet.* **1984**, *16*, 1175−1186.
(10) Smith, G. P. Laser Pyrolysis Studies of OH Reaction Rates with Several Butenes at 1200 K. *Int. J. Chem. Kinet.* **1987**, *19*, 269−276.
(11) Tully, F. P. Hydrogen-Atom Abstraction from Alkenes by OH, Ethene and 1-butene. *Chem. Phys. Lett.* **1988**, *143*, 510−514.
(12) Sims, I. R.; Smith, I. W. M.; Bocherel, P.; Defrance, A.; Travers, D.; Rowe, B. R. Ultra-Low Temperature Kinetics of Neutral−neutral Reactions: Rate Constants for the Reactions of OH Radicals with Butenes Between 295 and 23 K. *J. Chem. Soc., Faraday Trans.* **1994**, *90*, 1473−1478.
(13) Vakhtin, A. B.; Lee, S.; Heard, D. E.; Smith, I. W. M.; Leone, S. R. Low-Temperature Kinetics of Reactions of the OH Radical with Propene and 1-Butene Studied by a Pulsed Laval Nozzle Apparatus Combined with Laser-Induced Fluorescence. *J. Phys. Chem. A* **2001**, *105*, 7889−7895.
(14) Canosa-Mas, C. E.; King, M. D.; Mcdonnell, L.; Wayne, R. P. An Experimental Study of the Gas-Phase Reactions of the NO_3 Radical with Pent-1-ene, Hex-1-ene and Hept-1-ene. *Phys. Chem. Chem. Phys.* **1999**, *1*, 2681−2685.
(15) Piqueras, M. C.; Crespo, R.; Nebot-Gil, I.; Tomás, F. Thermochemical Analysis of the OH+C_2H_4 → C_2H_4OH Reaction Using Accurate Theoretical Methods. *J. Mol. Struct. (THEOCHEM)* **2001**, *537*, 199−212.
(16) Atkinson, R. Gas-phase Tropospheric Chemistry of Organic Compounds. *J. Phys. Chem. Ref. Data* **1994**, *24*, 1−216 Monograph 2.
(17) Atkinson, R. Kinetics and Mechanisms of the Gas-Phase Reactions of the Hydroxyl with Organic Compounds. *J. Phys. Chem. Ref. Data* **1989**, 1−246 Monograph 1.
(18) Atkinson, R. Kinetics and Mechanisms of the Gas-Phase Reactions with the Hydroxyl Radical with Organic Compounds Under Atmospheric Conditions. *Chem. Rev.* **1986**, *86*, 69−201.
(19) Papagni, C.; Arey, J.; Atkinson, R. Rate Constants for the Gas-Phase Reactions of OH Radicals with a Series of Unsaturated Alcohols. *Int. J. Chem. Kinet.* **2001**, *33*, 142−147.
(20) Cometto, P. M.; Dalmasso, P. R.; Taccone, R. A.; Lane, S. I.; Oussar, F.; Daële, V.; Mellouki, A.; Le Bras, G. Rate Coefficients for the Reaction of OH with a Series of Unsaturated Alcohols Between 263 and 371 K. *J. Phys. Chem. A* **2008**, *112*, 4444−4450.
(21) Du, B.; Feng, C.; Zhang, W.; Mu, L. Theoretical Study on the Mechanism for the Reaction of OH with $CH_2CHCH_2CH_2OH$. *Chem. Phys.* **2010**, *367*, 52−61.
(22) Barbosa, T. S.; Nieto, J. D.; Cometto, P. M.; Lane, S. I.; Bauerfeldt, G. F.; Arbilla, G. Theoretical Calculations of the Kinetics of the OH Reaction with 2-methyl-2-propen-1-ol and its Alkene Analogue. *RSC Adv.* **2014**, *4*, 20830−20840.
(23) Levine, I. N. *Quantum Chemistry*; Prentice Hall: NJ, 2000.
(24) Becke, A. D. A New Mixing of Hartree-Fock and Local Density-Functional Theories. *J. Chem. Phys.* **1993**, *98*, 1372−1377.
(25) Dunning, T. H. Gaussian Basis Sets for Use in Correlated Molecular Calculations. I. The Atoms Boron through Neon and Hydrogen. *J. Chem. Phys.* **1989**, *90*, 1007−1023.
(26) Lin, R. J.; Wu, C. C.; Jang, S.; Li, F. Y. Variation of Reaction Dynamics for OH Hydrogen Abstraction from Glycine Between Ab Initio Levels of Theory. *J. Mol. Model.* **2010**, *16*, 175−182.
(27) Maroulis, G. Evaluating the Performance of DFT Methods in Electric Property Calculations: Sodium Chloride as a Test Case. *Rep. Theor. Chem.* **2013**, *2*, 1−8.
(28) Guadarrama, P.; Soto-Castro, D.; Rodríguez-Otero, J. Performance of DFT Hybrid Functionals in the Theoretical Treatment of H-Bonds: Analysis Term-by-Term. *Int. J. Quantum Chem.* **2008**, *108*, 229−237.
(29) Fukui, K. A. A Formulation of the Reaction Coordinate. *J. Phys. Chem.* **1970**, *74*, 4161−4163.
(30) Cramer, C. J. *Essentials of Computational Chemistry Theories and Models*; John Wiley and Sons: New York, 2004.
(31) Frisch, M. J.; Trucks, G. W.; Schlegel, H. B.; Scuseria, G. E.; Robb, M. A.; Cheeseman, J. R.; Scalmani, G.; Barone, V.; Mennucci, B.; Petersson, G. A.; et al. *Gaussian 09*, revision A.02; Gaussian, Inc.: Wallingford, CT, 2009.
(32) Truhlar, D. G.; Garret, B. C. *Annu. Rev. Phys. Chem.* **1984**, *35*, 159−189.
(33) Zhu, L.; Hase, W. L. Comparison of Models for Calculating the RRKM Unimolecular Rate Constant k(E,J). *Chem. Phys. Lett.* **1990**, *175*, 117−124.
(34) Greenwald, E. E.; North, S. W.; Georgievskii, Y.; Klippenstein, S. J. A Two Transition State Model for Radical − Molecule Reactions: A Case Study of the Addition of OH to C_2H_4. *J. Phys. Chem. A* **2005**, *109*, 6031−6044.
(35) Singleton, D. L.; Cvetanovic, R. J. Temperature Dependence of the Reaction of Oxygen Atoms with Olefins. *J. Am. Chem. Soc.* **1976**, *98*, 6812−6819.
(36) Alvarez-Idaboy, J. R.; Mora-Diez, N.; Vivier-Bunge, A. A Quantum Chemical and Classical Transition State Theory Explanation of Negative Activation Energies in OH Addition to Substituted Ethenes. *J. Am. Chem. Soc.* **2000**, *122*, 3715−3520.
(37) Alvarez-Idaboy, J. R.; Mora-Diez, N.; Boyds, R. J.; Vivier-Bunge, A. On the Importance of Pre-Reactive Complexes in Molecule-Radical Reactions: Hydrogen Abstraction from Aldehydes by OH. *J. Am. Chem. Soc.* **2001**, *123*, 2018−2024.
(38) Francisco-Márquez, M.; Alvarez-Idaboy, J. R.; Galano, A.; Vivier-Bunge, A. On the Role of s-cis Conformers in the Reaction of Dienes with OH Radicals. *Phys. Chem. Chem. Phys.* **2004**, *6*, 2237−2244.

DOI: 10.1021/jp512544x
J. Phys. Chem. A 2015, 119, 3171−3180